Published in final edited form as:
Math Biosci. 2015 March ; 261: 48–61. doi:10.1016/j.mbs.2014.11.004.

Analysis of a compartmental model of amyloid beta production, irreversible loss and exchange in humans

Donald L. Elbert[1,*], **Bruce W. Patterson**[2], and **Randall J. Bateman**[3,4,5,*]

[1] Department of Biomedical Engineering, Washington University in St. Louis, St. Louis, MO 63130, USA

[2] Department of Medicine, Washington University School of Medicine, St. Louis, MO 63110, USA

[3] Department of Neurology, Washington University School of Medicine, St. Louis, MO 63110, USA

[4] Charles F. and Joanne Knight Alzheimer's Disease Research Center, Washington University School of Medicine, St. Louis, MO 63110, USA.

[5] Hope Center for Neurological Disorders, Washington University School of Medicine, St. Louis, MO 63110, USA

Abstract

Amyloid beta (Aβ) peptides, and in particular Aβ42, are found in senile plaques associated with Alzheimer's disease. A compartmental model of Aβ production, exchange and irreversible loss was recently developed to explain the kinetics of isotope-labeling of Aβ peptides collected in cerebrospinal fluid (CSF) following infusion of stable isotope-labeled leucine in humans. The compartmental model allowed calculation of the rates of production, irreversible loss (or turnover) and short-term exchange of Aβ peptides. Exchange of Aβ42 was particularly pronounced in amyloid plaque-bearing participants. In the current work, we describe in much greater detail the characteristics of the compartmental model to two distinct audiences: physician-scientists and biokineticists. For physician-scientists, we describe through examples the types of questions the model can and cannot answer, as well as correct some misunderstandings of previous kinetic analyses applied to this type of isotope labeling data. For biokineticists, we perform a system identifiability analysis and a sensitivity analysis of the kinetic model to explore the global and local properties of the model. Combined, these analyses motivate simplifications from a more comprehensive physiological model to the final model that was previously presented. The analyses clearly demonstrate that the current dataset and compartmental model allow determination with confidence a single ‘turnover’ parameter, a single ‘exchange’ parameter and a single ‘delay’

[*]**Co-corresponding authors: Donald L. Elbert** Washington University in St. Louis, Department of Biomedical Engineering One Brookings Dr., Campus Box 1097 St. Louis, MO 63130 **elbert@wustl.edu Randall J. Bateman** Washington University School of Medicine, Department of Neurology 660 South Euclid Avenue, Campus Box 8111 St. Louis, MO 63110 batemanr@wustl.edu.

parameter. When combined with CSF concentration data for the Aβ peptides, production rates may also be obtained.

Keywords

amyloid beta; Alzheimer's Disease; amyloidosis; kinetics; compartmental model; sensitivity analysis; identifiability

1. Introduction

The amyloid hypothesis posits a direct link between amyloid β-peptide (Aβ peptide) turnover kinetics and Alzheimer's Disease (AD) [1]. The Aβ precursor protein (APP), produced in high amounts by neurons, is known to be degraded by different enzymes [2]. The enzyme β-secretase cleaves APP to produce the C99 peptide. C99 is then further processed by γ-secretase to produce Aβ peptides of different lengths (*e.g.* Aβ38, Aβ40, Aβ42, where the number indicates the number of amino acids in the peptide). Aβ peptides are able to self-aggregate, with Aβ42 being more prone to formation of large aggregates [3], and the major constituent of senile plaques [4]. Although the amyloid hypothesis is well-supported by a number of lines of evidence, the roles of Aβ peptide and other proteins (*e.g.* Apolipoprotein E) that result in the formation of senile plaques are only beginning to be deciphered [1].

A promising approach to characterize the kinetics of Aβ production and clearance in humans relies on *in vivo* labeling of Aβ peptides during protein translation via infusion of stable isotope-labeled amino acids, stable isotope labeling kinetics (SILK) [5]. The fraction of isotope-labeled Aβ is measured at timed intervals in cerebrospinal fluid (CSF) collected at the lumbar subarachnoid space. The traditional method to estimate rates of irreversible loss of Aβ peptides from the CNS is analysis of the terminal slopes of isotopic enrichment time course curves evaluated on log-normal plots. This analysis method yields a measure that is referred to herein as the monoexponential fractional clearance rate (monoexponential FCR) [6]. Previous results demonstrated decreased monoexponential FCR of both Aβ40 and Aβ42 in late-onset AD [7]. However, the monoexponential FCR should not be confused with the *true underlying fractional clearance rate*, which may be difficult to determine in complicated systems. The true fractional clearance rate is the rate of irreversible loss of a product divided by the pool size of the product. To avoid confusion, we use the term *fractional turnover rate* or *FTR*, which has the same meaning as the true fractional clearance rate. The FTR is also equal to the sum of all of the rate constants describing routes of irreversible loss. The fractional synthesis rate (FSR) was determined by fitting a line to the upslope of the isotopic enrichment time course curve. FSR is defined as “the rate of incorporation from precursor to product divided by the pool size of the product” [6]. Thus, FSR is distinct from our desired quantity, called here the *production rate constant*, which is the rate of incorporation from precursor to product divided by the pool size of the *precursor*. The FSR and monoexponential FCR analysis methods were acknowledged to have limitations, in that they imposed a simple one-compartment model on a complicated system [8]. However, more physiologically relevant models had not yet been developed.

In a recent publication, we introduced a physiologically relevant multi-compartmental model to distinguish carriers of presenilin-1 or presenilin-2 mutations that are the active enzymatic components of γ-secretase and result in onset of AD at younger ages than non-mutation carriers (familial autosomal dominant AD) [9]. The main strength of the new model is that the rates of production, transport, reversible and irreversible loss of APP, C99, and the Aβ peptides may be estimated by fitting the model to the entire time course of the isotopic enrichment data while also accounting for the Aβ peptide concentrations in CSF. The model successfully detected an increase in the rate of production of Aβ42 relative to Aβ40 in human subjects with presenilin mutations, consistent with results *in vitro* and in mice [10]. Increased FTR of soluble Aβ42 relative to Aβ40 were also detected in participants known to have senile plaques demonstrated by positron emission tomography (PET) using Pittsburgh Compound B (PIB). The previous observation of decreased monoexponential FCR of Aβ42 in late onset AD was re-interpreted in the context of amyloid positive mutation carriers when the full enrichment time courses were fit to the compartmental model [7]. From the analysis of Aβ isoforms in mutation carriers, it was concluded that the data actually reflected *increased* irreversible loss of soluble Aβ42 relative to Aβ40. Faster irreversible loss in combination with exchange of Aβ42 with higher order structures (*e.g.* aggregates, micelles, or the surface of pre-existing plaques) resulted in a ‘slower’ terminal exponential tail.

The compartmental model answered several questions concerning the amyloid hypothesis. However, the previous publication on the compartmental model did not discuss the *identifiability* of particular parameters [11, 12]. In this work, the identifiability of the different parameters in the compartmental model is described via a parameter sensitivity analysis. Analysis of the steady state of the model also revealed a potential mechanism for the decrease in the CSF concentration of Aβ42 in Alzheimer's disease [13]. Additionally, we address some issues concerning the nature of isotope labeling experiments that have been debated in the literature [14].

2. Methods

Experimental methods for isotopic labeling of Aβ peptides and measurement of their concentrations in CSF are described in a separate publication [9]. Systems identifiability analysis and sensitivity analysis were performed as described in the text.

3. Theory/calculation

A compartmental model was constructed to describe Aβ peptide-labeling data (Figure 1)[9]. The brain was modeled as a reactor that produces APP from a pool of isotopically labeled plasma leucine with a zero-order rate constant k_{APP}. APP is then processed to become C99 (first order rate constant k_{C99}) or other products (first order rate constant v_{APP}). C99 is further processed to produce soluble Aβ38, Aβ40, or Aβ42 and other products (*e.g.* Aβ peptides of other lengths) with first order rate constants k_{Ab38}, k_{Ab40}, k_{Ab42} and v_{C99}, respectively. Irreversible loss of each soluble Aβ peptide from the brain compartment that does *not* result in transport to CSF (*e.g.* insoluble deposition, degradation, or transfer across the blood-brain barrier) is modeled as first order processes with rate constants v_{38}, v_{40}, v_{42} for the respective Aβ peptides. The soluble Aβ peptides may also enter a reversible, short-

term exchange compartment while in the brain (k_{ex38}, k_{ex40} and k_{ex42} for entry into and k_{ret38}, k_{ret40} and k_{ret42} for return from the respective compartments). Transport of soluble Aβ peptides out of the brain into the CSF is modeled as a first order process with rate constants k_{CSF38}, k_{CSF40} and k_{CSF42}, respectively. In practice, k_{ret38}, k_{ret40} and k_{ret42} were assumed to be identical and were called simply $k_{ret}$and k_{CSF38}, k_{CSF40} and k_{CSF42} were assumed to be equal (with justifications to follow). Transport within the CSF is modeled by three compartments with equal first order exit rate constants (k_{delay} or sometimes k_{del}), which are assumed to be the same for all Aβ peptides. The lumbar CSF concentration and isotopic labeling of each Aβ peptide was measured and used in the model as the target concentration and labeling fraction in each peptide's third delay compartment. Appendix A describes the development of the model, starting from a mathematical model with the minimal structure necessary and sufficient to account for the shape of the isotopic enrichment time courses, and progressing through steps that transformed this starting model into a physiologically relevant model. The model in Appendix A was simplified compared to that shown in Figure 1, due to our empirical observation of identifiability issues for some of the parameters. To address identifiability concerns rigorously, the exact solution to the rate equations for the full model shown in Figure 1 was calculated and is described below. A more detailed description of the exact solution is found in Appendix B.

3.1. APP labeling kinetics during infusion of isotope-labeled leucine

Prior to the addition of labeled leucine, a steady state was presumed whereby the rate of production of the unlabeled protein (k_{APP}) was equal to the rate of conversion to C99 ($-k_{C99}$ *x* c_{APP}) or other products ($-v_{APP}$ *x* c_{APP}). A steady state pool size of APP (concentration of APP multiplied by compartment volume) was assumed throughout the labeling experiment, thus:

$$\frac{dc_{APP,SS}}{dt} = k_{APP} - (k_{C99} + v_{APP})\, c_{APP,SS} = 0 \quad \text{Eq(3.1.1)}$$

or,

$$c_{APP,SS} = \frac{k_{APP}}{k_{C99} + v_{APP}} \quad \text{Eq(3.1.2)}$$

To simplify the analysis, the fraction of isotopically labeled leucine in plasma was taken to be the average value during the labeling phase, *f*. Rates of change in the pool size of unlabeled APP (c_{APP}) and labeled APP (c_{APPL}) during the infusion phase are thus:

$$\frac{dc_{APP}}{dt} = k_{APP}\,(1 - f) - (k_{C99} = v_{APP})\, c_{APP} \quad \text{Eq(3.1.3)}$$

and

$$\frac{dc_{APPL}}{dt} = k_{APP} f - (k_{C99} + v_{APP})\, c_{APPL} \quad \text{Eq(3.1.4)}$$

These equations imply that labeled leucine is added to tRNA proportional to the fraction *f* of labeled leucine, not the tracer-to-tracee ratio (TTR). The fraction *f* is [Labeled leucine]/([Unlabeled Leucine] + [Labeled Leucine]), while the TTR is [Labeled leucine]/[Unlabeled Leucine]. The fraction *f* has been shown to be the appropriate model for protein synthesis [15], and differs from the previous analysis method that used the TTR [7], although at the limit of low enrichment this is a minor difference. The use of TTR versus fractional labeling is further described in Appendix C.

The equations are solved:

$$c_{APP}=c_{APP0}e^{-(k_{C99}+v_{APP})t}+\frac{k_{APP}}{(k_{C99}+v_{APP})}(1-f)\left(1-e^{-(k_{C99}+v_{APP})t}\right) \quad \text{Eq(3.1.5)}$$

and

$$c_{APPL}=c_{APPL0}e^{-(k_{C99}+v_{APP})t}+\frac{k_{APP}}{(k_{C99}+v_{APP})}f\left(1-e^{-(k_{C99}+v_{APP})t}\right) \quad \text{Eq(3.1.6)}$$

The initial conditions at the moment of addition of labeled amino acid were:

$$c_{APP0}=\frac{k_{APP}}{(k_{C99}+v_{APP})} \quad \text{Eq(3.1.7)}$$

and

$$c_{APPL0}=0 \quad \text{Eq(3.1.8)}$$

The solutions appropriate for these initial conditions are:

$$c_{APP}=\frac{k_{APP}}{(k_{C99}+v_{APP}}\left(1-f\left(1-e^{-(k_{C99}+v_{APP})t}\right)\right) \quad \text{Eq(3.1.9)}$$

and

$$c_{APPL}=\frac{k_{APP}}{(k_{C99}+v_{APP})}f\left(1-e^{-(k_{C99}+v_{APP})t}\right) \quad \text{Eq(3.1.10)}$$

If the rates of production and irreversible loss of APP do not change during the course of the labeling experiment, the pool sizes of labeled plus unlabeled protein will equal the original steady state pool size of protein:

$$c_{APP,ss}=c_{APP}+c_{APPL} \quad \text{Eq(3.1.11)}$$

Stated another way, the pool size of unlabeled protein must decline because a fraction of the tRNAs are loaded with the labeled amino acid.

The fractional labeling of APP (p_{APPL}) is obtained by dividing equation 3.1.10 by equation 3.1.2:

$$p_{APPL}=\frac{c_{APPL}}{c_{APP,ss}}=\frac{c_{APPL}}{k_{APP}/\left(k_{C99}+v_{APP}\right)}=f\left(1-e^{-\left(k_{C99}+v_{APP}\right)t}\right) \quad \text{Eq(3.1.12)}$$

The same result would be obtained by dividing the rate equation for c_{APPL} by the steady state concentration of APP and solving this differential equation:

$$\begin{aligned}&\frac{d\left(\frac{c_{APPL}}{c_{APP,ss}}\right)}{dt}=\frac{dp_{APPL}}{dt}=\frac{k_{APP}f-\left(k_{C99}+v_{APP}\right)c_{APPL}}{c_{APP,ss}}\\&=\frac{k_{APP}f}{k_{APP}/\left(k_{C99}+v_{APP}\right)}-\left(k_{C99}+v_{APP}\right)p_{APPL}\\&=\left(k_{C99}+v_{APP}\right)\left(f-p_{APPL}\right)\end{aligned} \quad \text{Eq(3.1.13)}$$

Notice that the 'rate of appearance' of labeled APP in Eq(3.1.12) does not depend on the parameter k_{APP}. Basic kinetic intuition would suggest that the slope of the initial portion of the labeling curve should equal the APP synthesis rate constant k_{APP}. This would be true if concentrations or pool sizes were measured, but not if TTR or fractional labeling are measured. To see this, the exponential terms in the equations for c_{APPL} and p_{APPL} are expanded as Taylor series in time. Assuming very short times, the terms in t^2 and higher may be neglected:

$$\begin{aligned}c_{APPL}&=\frac{k_{APP}}{\left(k_{C99}+v_{APP}\right)}f\left(1-\left(1-\left(k_{C99}+v_{APP}\right)t+\tfrac{1}{2}\left(\left(k_{C99}+v_{APP}\right)t\right)^2+\ldots\right)\right)\\&\cong fk_{APP}t\end{aligned} \quad \text{Eq(3.1.14)}$$

However, for fractional labeling:

$$\begin{aligned}p_{APPL}&=f\left(1-\left(1-\left(k_{CPP}+v_{APP}\right)t+\tfrac{1}{2}\left(\left(k_{C99}+v_{APP}\right)t\right)^2\right)\right)\\&\cong f\left(k_{CPP}+v_{APP}\right)t\end{aligned} \quad \text{Eq(3.1.15)}$$

Although this section specifically described APP production and clearance rates, the conclusions are valid for any one compartment model. The initial slope of a labeling curve for a one-compartment model yields a measure of the irreversible loss rate constant and not its production rate constant. However, later it will be shown that the upslope of a labeling curve for a system described by a multicompartment model is more complicated.

3.2. APP labeling kinetics following removal of isotope-labeled leucine

At the end of the labeling period, the infusion of labeled amino acid ceases. The labeled fraction of isotope-labeled leucine in plasma drops rapidly and is well-described by a bi-exponential decay:

$$f=f_0\left(\alpha e^{-q_m t}+\beta e^{-q_r t}\right) \quad \text{Eq(3.2.1)}$$

where f_0 is the fraction of labeled amino acid in plasma during the labeling period. For compactness, t = 0 in this equation corresponds to the *end* of the labeling period. The sum of the parameters α and β is one. The parameters α and q_m tend to be large and presumably represent rapid clearance of the labeled amino acid throughout the body. The parameters β and q_r tend to be much smaller and likely represent reappearance of labeled leucine in

plasma due to exchange of labeled plasma amino acid with non-plasma spaces and/or incorporation into and subsequent degradation of rapidly turning over proteins throughout the body.

At the end of the labeling period, labeled APP had a pool size of $c_{APPL,end}$. The rate equation for labeled APP Eq(3.1.4) is solved with the new expression for f and with initial condition $c_{APPL}(0) = c_{APPL,end}$:

$$c_{APPL}=k_{APP}f_0\left(\frac{\alpha}{k_{C99}+v_{APP}-q_m}e^{-q_m t}+\frac{\beta}{k_{C99}+v_{APP}-q_r}e^{-q_r t}\right) + \left(c_{APPL,end}-k_{APP}f_0\left(\frac{\alpha}{k_{C99}+v_{APP}}-q_m+\frac{\beta}{k_{C99}+v_{APP}-q_r}\right)\right)e^{-(k_{C99}+v_{APP})t} \quad \text{Eq(3.2.2)}$$

The pool size of APP at the end of the labeling period is obtained from equation (3.1.10):

$$c_{APPL,end}=\frac{k_{APP}}{k_{C99}+v_{APP}}f\left(1-e^{-(k_{C99}+v_{APP})t_{end}}\right) \quad \text{Eq(3.2.3)}$$

where t_{end} is the length of the labeling period.

Dividing by the pool size of APP at steady state, the fractional labeling of APP after removal of labeled amino acid is:

$$p_{APPL}=(k_{C99}+v_{APP})\,f_0\left(\frac{\alpha\left(e^{-q_m t}-e^{-(k_{C99}+v_{APP})t}\right)}{k_{C99}+v_{APP}-q_m}+\frac{\beta\left(e^{-q_r t}-e^{-(k_{C99}+v_{APP})t}\right)}{k_{C99}+v_{APP}-q_r}\right)+p_{APPL,end}e^{-(k_{C99}+v_{APP})t} \quad \text{Eq(3.2.4)}$$

The first term on the right hand side represents new synthesis of labeled APP due to residual labeled amino acid. If the ‘new synthesis’ term is neglected, then a semilog-y plot would yield:

$$ln\,(p_{APPL})=ln\left(p_{APPL,end}\right)-(k_{C99}+v_{APP})\,t \quad \text{Eq(3.2.5)}$$

with slope of –(k_{C99} + v_{APP}). This illustrates the fact that the downslope of a one compartment model would yield an approximation of the rate constants describing ‘clearance’ but no information about rate constants of ‘production’ (the full model described below does not neglect new synthesis, unlike simple fits of monoexponential curves to the downslope of the labeling curve).

3.3. Labeling kinetics in other compartments

The rate equation that describes production of labeled C99 during the labeling phase is:

$$\frac{dc_{C99L}}{dt}=k_{C99}c_{APPL}-(k_{Ab38}+k_{Ab40}+k_{Ab42}+v_{C99})\,c_{C99L} \quad \text{Eq(3.3.1)}$$

The rate constants k_{Ab38}, k_{Ab40}, and k_{Ab42} govern the rate of production of Aβ38, Aβ40 and Aβ42, respectively. The rate constant v_{C99} describes all other irreversible losses of C99,

including production of Aβ peptides of other molecular weights. For compactness, $k_{Ab} = k_{Ab38} + k_{Ab40} + k_{Ab42} + v_{C99}$.

The rate equations for all three Aβ peptides are similar and will be elaborated for Aβ42 only. The rate equation for labeling kinetics of soluble Aβ42 in the 'brain' is:

$$\frac{dc_{Ab42L}}{dt} = k_{Ab42} c_{C99L} - (v_{42} + k_{CSF} + k_{ex42})\, c_{Ab42L} + k_{ret42} c_{Ab42exL} \quad \text{Eq(3.3.2)}$$

The parameter k_{Ab42} represents production of Aβ42 from C99 by the action of γ-secretase, v_{42} describes irreversible loss of Aβ42 from the soluble brain compartment by means other than transfer to CSF, k_{CSF} describes irreversible loss into CSF, k_{ex42} describes entry into an exchange compartment, k_{ret42} describes return of Aβ42 from the exchange compartment to the 'brain' compartment, and $c_{Aβ42exL}$ is the pool size of labeled Aβ42 in the exchange compartment.

The kinetics of entry/exit of labeled Aβ42 into/from the exchange compartment are described by the rate equation:

$$\frac{dc_{Ab42exL}}{dt} = k_{ex42} c_{Ab42L} - k_{ret42} c_{Ab42exL} \quad \text{Eq(3.3.3)}$$

We hypothesize that the 'exchange' compartment represents a reversible interaction with higher order structures, perhaps with the surface of amyloid plaques or oligomers (see reference 9 and Appendix A for additional discussion) [9]. In contrast, permanent or even slowly reversible assimilation into stable plaques would lead to an increase in the parameter v_{42}, because the labeled Aβ would not return to the soluble form during the time course of the experiment. This would thus be indistinguishable from other mechanisms of irreversible loss of Aβ42.

The rate equations for the three CSF delay compartments are:

1. First CSF delay compartment:

$$\frac{dc_{Ab42d1L}}{dt} = k_{CSF} c_{Ab42L} - k_{del} c_{Ab42d1L} \quad \text{Eq(3.3.4)}$$

2. Second CSF delay compartment:

$$\frac{dc_{Ab42d2L}}{dt} = k_{del} (c_{Ab42d1L} - c_{Ab42d2L}) \quad \text{Eq(3.3.5)}$$

3. Third CSF delay compartment:

$$\frac{dc_{Ab42d3L}}{dt} = k_{del} (c_{Ab42d2L} - c_{Ab42d3L}) \quad \text{Eq(3.3.6)}$$

The system of differential equations in terms of fractional labeling may be written as:

$$\begin{bmatrix} \dot{p}_{APPL} \\ \dot{p}_{C99L} \\ \dot{p}_{Ab42L} \\ \dot{p}_{Ab42exL} \\ \dot{p}_{Ab42d1L} \\ \dot{p}_{Ab42d2L} \\ \dot{p}_{Ab42d3L} \end{bmatrix} = \begin{bmatrix} -(k_{C99}+v_{APP}) & 0 & 0 & 0 & 0 & 0 & 0 \\ k_{Ab} & -k_{Ab} & 0 & 0 & 0 & 0 & 0 \\ 0 & (v_{42}+k_{CSF}) & -(v_{42}+k_{CSF}+k_{ex42}) & k_{ex42} & 0 & 0 & 0 \\ 0 & 0 & k_{ret42} & -k_{ret42} & 0 & 0 & 0 \\ 0 & 0 & k_{del} & 0 & -k_{del} & 0 & 0 \\ 0 & 0 & 0 & 0 & k_{del} & -k_{del} & 0 \\ 0 & 0 & 0 & 0 & 0 & k_{del} & -k_{del} \end{bmatrix} \begin{bmatrix} p_{APPL} \\ p_{C99L} \\ p_{Ab42L} \\ p_{Ab42exL} \\ p_{Ab42d1L} \\ p_{Ab42d2L} \\ p_{Ab42d3L} \end{bmatrix} + \begin{bmatrix} (k_{C99}+v_{APP})\, f \\ 0 \\ 0 \\ 0 \\ 0 \\ 0 \\ 0 \end{bmatrix} \quad \text{Eq(3.3.7)}$$

and may be solved directly. The solution during the post-labeling phase is:

$$\begin{aligned} p_{Ab42d3L} = {k_{del}}^3 \times & \left(\begin{array}{l} X^p \left(\frac{\left(e^{-k_{Ab}t} - \left(1+t\left(k_{del}-k_{Ab}\right)+\frac{1}{2}t^2\left(k_{del}-k_{Ab}\right)^2\right)e^{-k_{del}t}\right)}{\left(k_{del}-k_{Ab}\right)^3} - \phi_3 + \frac{k_{Ab}+(Q+R)}{2R}\left(\phi_3 - v_3\right)\right) \\ +Y_p \left(\frac{\left(e^{-k_{C99}t} - \left(1+t\left(k_{del}-k_{C99}\right)+\frac{1}{2}t^2\left(k_{del}-k_{C99}\right)^2 e^{-k_{del}t}\right)\right)}{\left(k_{del}-k_{C99}\right)^3} - \phi_3 + \frac{k_{C99}+(Q+R)}{2R}\left(\phi_3 - v_3\right)\right) \\ +Z_p \left(\mu - \phi_3 + \frac{q_m+(Q+R)}{2R}\left(\phi_3 - v_3\right)\right) + {Z'}_p \left(\rho - \phi_3 + \frac{q_r+(Q+R)}{2R}\left(\phi_3 - v_3\right)\right) \\ +p_{Ab42L,end}\phi_3 + \frac{\left({p'}_{Ab42L,end} - (Q+R)p_{Ab42L,end}\right)}{2R}\left(\phi_3 - v_3\right) \end{array} \right) \\ & + \left(p_{Ab42d3L,end} + k_{del}p_{Ab42d2L,end}t + {k_{del}}^2 p_{Ab42d1L,end}\frac{1}{2}t^2\right) e^{-k_{del}t} \end{aligned} \quad \text{Eq(3.3.8)}$$

with the full derivation shown in Appendix B and solution with definitions of coefficients summarized in Appendix D for easy reference. For the labeling phase, the same equation applies but with $f = f_0$, meaning that q_r and q_m in equation 3.2.1 are equal to zero, and fractional labeling is zero at $t = 0$ for all peptides. The predicted time course of labeling in each compartment is shown in Figure 3.

Equation (3.3.8) describes the shape of the isotopic enrichment time course curve according to this compartmental model. An important conclusion is that the rate constant for production of Aβ42 ($k_{Aβ42}$) does not appear in these equations except through its inclusion in k_{Ab}. Thus, any impact that $k_{Aβ42}$ has on Aβ labeling kinetics would only be manifest if this caused an increase in the rate of turnover of C99. If increases in secretase activity to produce

Aβ42 are exactly balanced by decreases in production of other Aβ isoforms, then the model predicts that increases in the rate of production of Aβ42 would not be detectable by an isotope labeling experiment alone. However, as will be shown by a steady state analysis, the rate of production of Aβ peptides may be calculated by using both Aβ42 isotope labeling kinetics and CSF Aβ42 concentration data.

3.4 Fractional synthesis rate (FSR) and fractional clearance rate (FCR) in multicompartment systems

The goal of the experimental studies was to determine the rate constants for the production (k_{38}, k_{40} and k_{42}) and irreversible loss (v_{38}, v_{40} and v_{42}) of the Aβ peptides. In the former case, this may sometimes be stated as determining the 'production rates of the Aβ peptides'. Because the Aβ peptides have a common precursor (C99), the production rate constants are in fact the true determinants of the production rates. Similarly, it may be stated that the 'clearance rates' are of interest. However, this is much less precise, because these rates (or fluxes, both with units of mass/time or concentration/time) depend on the pool size/concentration of each Aβ peptide, which differ greatly. In fact, the kinetic measures that allow meaningful comparisons of irreversible loss between the different Aβ isoforms are the 'clearance rate constants' or 'irreversible loss rate constants'.

Because the models are at steady state, the production rate and irreversible loss rate must be equal. Thus, only one rate is required, the 'turnover' rate [16, 17]. The turnover rate divided by the concentration or pool size of the product is the fractional turnover rate (FTR), which is equal to the irreversible loss rate constant. The 'fractional synthesis rate' is the rate of appearance of labeled product divided by the pool size or concentration of the *product* [6], which is the same as dividing the turnover rate by the product pool size. Thus, the fractional synthesis rate is theoretically the same as the FTR (*i.e*. true FCR) and the irreversible loss rate constant. However, the 'FSR' often refers to the *method of estimating* the fractional turnover rate by fitting a line to the upslope of a curve and dividing the slope by the enrichment of the precursor. This method of estimating FTR is only accurate for systems well-described by single-compartment models. However, CSF Aβ kinetics are best described by a multi-compartmental model, and the 'FSR' that was previously applied to CSF Aβ kinetics [7, 14] may thus actually reflect changes in the *production rate constant*, one of the two quantities of interest.

Figure 4 illustrates these concepts. A simple model is simulated (Figure 4A&B), in which a precursor with constant concentration during a nine-hour labeling phase may produce two products with different irreversible loss rate constants (v_1 & v_2). However, Figure 4A is simply two parallel one-compartment models. The production rate constants (k_1 & k_2) are varied. The FSR is estimated from the initial slope of the product labeling curves (first three data points), while the FCR is the monoexponential slope from 24-36 h. As the production rate constants vary, the labeling curves do not change in the one-compartment models. However, both the FSR and FCR provide good estimates of the fractional turnover rate (*i.e*. irreversible loss rate constants v_1 & v_2). Although the production rate constants appear to be indecipherable from the data, they are simply:

$$k_1 = \frac{v_1 \times c_{\text{product1},SS}}{c_{\text{precursor},SS}} = \frac{FCR_{\text{product1}} \times c_{\text{product1},SS}}{c_{\text{precursor},SS}} = \frac{FSR_{\text{product1}} \times c_{\text{product1},SS}}{c_{\text{precursor},SS}} \quad \text{Eq(3.4.1)}$$

$$k_2 = \frac{v_2 \times c_{\text{product2},SS}}{c_{\text{precursor},SS}} = \frac{FCR_{\text{product2}} \times c_{\text{product2},SS}}{c_{\text{precursor},SS}} = \frac{FSR_{\text{product2}} \times c_{\text{product2},SS}}{c_{\text{precursor},SS}} \quad \text{Eq(3.4.2)}$$

where $c_{product\ x,SS}$ is the steady state concentration of product x.

In Figure 4C, the model is expanded into a multi-compartmental model, where precursor A is at a constant concentration during the labeling phase, and produces precursor B, which then splits to produces products 1 & 2. The rate constant k_f has no impact on the labeling curve, but could be calculated as:

$$k_f = \frac{(k_1 + k_2) \times c_{\text{precursorB},SS}}{c_{\text{precursorA},SS}} \quad \text{Eq(3.4.3)}$$

Changes in k_1 or k_2 also do not impact the labeling curve *as long as* $k_1 + k_2$ *remains constant* (Figure 4D). At constant $k_1 + k_2$, the shape of the labeling curve is only affected by v_1 & v_2 (Figure 4E). However, if $k_1 + k_2$ varies, the labeling curve shape is affected (Figure 4E). Thus, $k_1 + k_2$ is identifiable, but k_1 and k_2 are unidentifiable [11]. At constant v_1 & v_2, increases in $k_1 + k_2$ result in higher values for FSR and FCR, with the FCR coming closer to v_1 or v_2 (Figure 4F). The meaning of the measured value of the FSR for multicompartment systems is difficult to decipher, however it is clear that FSR is a measure of both production and irreversible loss, but only if an increase in production of the product causes a change in the irreversible loss of its precursor. Similar to the one-compartment model, the production rate constant is easily calculated if the irreversible loss rate constant is multiplied by the pool size/concentration of the product.

3.5. Steady state analysis

In addition to measurement of the fractional labeling of each of the Aβ peptides in the CSF, the concentration of each peptide in the CSF was measured by mass spectrometry. The concentrations of the Aβ peptides in CSF provided additional constraints on the parameters in the system. Although some diurnal variation in Aβ42 concentration in the CSF has been noted [18], the concentration in CSF at the start of the experiment was assumed to represent a steady state throughout the experiment.

To calculate pool size in each CSF compartment, the measured CSF concentration was multiplied by a typical CSF volume of 135 mL, and divided by 3 to account for three equal-volume CSF compartments in the model. The assumption that every participant had a CSF volume of 135 mL divided into 3 compartments seems strong but actually has little impact on the results. If the CSF concentrations of Aβ peptides were used instead of pool sizes, the results for all of the first-order rate constants would be identical, but the zero-order rate constant k_{APP} would simply be lower by a factor of 3/135. Because k_{APP} does not affect the

shape of the predicted isotope-labeling curve, use of either concentrations or pool sizes in fitting the labeling curves is justified.

According to the current model, the pool size of Aβ42 measured in the lumbar CSF is equal to the steady state pool size of Aβ42 in the third delay compartment. The steady state pool sizes of Aβ42 in each of the three delay compartments must be equal:

$$c_{Ab42,delay3,SS}=c_{Ab42,delay2,SS}=c_{Ab42,delay1,SS} \quad \text{Eq(3.5.1)}$$

Relative to the pool size of soluble Aβ42 in the brain, the pool size of Aβ42 in each delay compartment is predicted to be scaled by a factor k_{CSF}/k_{del}.

$$c_{Ab42,delay3,SS}=\frac{k_{CSF}}{k_{del}}c_{Ab42,brain,SS} \quad \text{Eq(3.5.2)}$$

The exchange compartment has no effect on the steady state pool size of soluble Aβ peptides in the brain or CSF. However, the pool size of the exchange compartment itself is:

$$c_{Ab42,exchange,SS}=k_{ex42}k_{ret42}c_{Ab42,brain,SS} \quad \text{Eq(3.5.3)}$$

Deposition into plaques or aggregates that do not return labeled Aβ42 on the time scale of the experiment would only impact the irreversible loss parameter, v_{42}. Thus, rates of deposition of Aβ42 into plaques can be estimated by comparing the difference between v_{42} and v_{40} , or between v_{42} and v_{38}, because Aβ38 and Aβ40 deposition into plaques is expected to be minimal [19].

After additional substitutions for the steady state concentrations of APP, C99, and Aβ peptides in the brain, the steady state concentrations in the CSF for each of the Aβ peptides is predicted to be:

$$c_{Ab38,delay3,SS}=\frac{k_{CSF}k_{C99}k_{APP}}{k_{del}\left(k_{C99}+v_{APP}\right)}\frac{k_{Ab38}}{\left(v_{38+v_{CSF}}\right)\left(k_{Ab38}+k_{Ab40}+k_{Ab42}+v_{C99}\right)} \quad \text{Eq(3.5.4)}$$

$$c_{Ab40,delay3,SS}=\frac{k_{CSF}k_{C99}k_{APP}}{k_{del}\left(k_{C99}+v_{APP}\right)}\frac{k_{Ab40}}{\left(v_{40+v_{CSF}}\right)\left(k_{Ab38}+k_{Ab40}+k_{Ab42}+v_{C99}\right)} \quad \text{Eq(3.5.5)}$$

$$c_{Ab42,delay3,SS}=\frac{k_{CSF}k_{C99}k_{APP}}{k_{del}\left(k_{C99}+v_{APP}\right)}\frac{k_{Ab42}}{\left(v_{42+v_{CSF}}\right)\left(k_{Ab38}+k_{Ab40}+k_{Ab42}+v_{C99}\right)} \quad \text{Eq(3.5.6)}$$

Overall, the model has 25 parameters:

$$k_{APP},v_{APP},k_{C99},v_{C99},k_{Ab38},k_{Ab40},k_{Ab42},v_{38},v_{40},v_{42},k_{ex38},k_{ex40},k_{ex42},k_{ret38},k_{ret40},$$
$$k_{ret42},k_{CSF38},k_{CSF40},k_{CSF42},k_{del38},k_{del40},k_{del42},SF_{38},SF_{40},SF_{42}$$

The last three parameters are scaling factors that were applied to the predicted labeling curve for each peptide. The scaling factors were found to improve the fit and may correct for systematic errors caused by variability in the standard curves used in the daily calibration of the mass spectrometers, or isotopic dilution between plasma leucine and APP production. The mean values of the scaling factors for all participants were 0.941 ± 0.08, 0.944 ± 0.08, and 0.937 ± 0.11 for Aβ38, Aβ40 and Aβ42, respectively, with no significant differences between groups. The model predictions of fractional labeling of the Aβ peptides in the CSF are linearly related to the scaling factors, and thus sensitivity to this parameter in isolation is uninformative.

As will be shown below, this model is 'system unidentifiable'. To reduce the number of parameters, the following assumptions were applied:

$$k_{CSF}=k_{CSF38}=k_{CSF40}=k_{CSF42}$$
$$k_{del}=k_{del38}=k_{del40}=k_{del42}$$
$$k_{ret}=k_{ret38}=k_{ret40}=k_{ret42}$$

The first two parameters (k_{CSF} and k_{del}) represent fluid flow processes and likely affect all three peptides equally. The third parameter (k_{ret}) could only be discerned for Aβ42 (see Appendix A) and may be different for Aβ38 and Aβ40. However, choosing the same value for k_{ret} for all three peptides allowed us to examine the extent of exchange of Aβ38 and Aβ40 relative to Aβ42. Exchange of Aβ38 and Aβ40 was found to be minimal and improved the fit of the model to the data in only a few subjects.

These assumptions reduced the model to 19 parameters. The CSF concentration size of each peptide is known, and because of steady state relationships Eq(3.5.4), Eq(3.5.5) and Eq(3.5.6), only 16 of the 19 parameters are independent. The choice of which three parameters are considered to be dependent is arbitrary, but the Aβ production rate constants $k_{Aβ38}$, $k_{Aβ40}$ and $k_{Aβ42}$ are easily calculated (see Appendix E) and a convenient choice.

3.6. Simplified model

Most of the Aβ isotope-labeling curves were found to be well-fit by a simple model consisting of 5 'delay' compartments arranged in series, with equal-valued rate constants for transfer between compartments, plus a single compartment turning over at a unique rate (see Appendix A). The data sets that could not be fit were primarily Aβ42 in subjects with significant amyloid plaque load as demonstrated by PET-PIB. The different morphology of the Aβ42 isotopic labeling time course compared to Aβ38 and Aβ40 in PIB-positive subjects is readily observed (*e.g.* see Figure 2A). The Aβ42 isotopic labeling time course from PIB-positive subjects was only well-fit when an exchange compartment was added to the model.

Although the exact solution presented above incorporates known biology and physiology, the current dataset was unable to independently identify all 16 rate constants in the model, for reasons that will be clear following the system identifiability and sensitivity analysis below. Thus, the model was further simplified using the following assumptions:

$$k_{C99}=k_{del}$$
$$v_{APP}=0$$
$$v_{C99}=\tfrac{1}{2}k_{del}$$
$$k_{Ab}=k_{Ab38}+k_{Ab40}+k_{Ab42}+v_{C99}=k_{del}$$
$$v_{40}=k_{CSF}$$
$$k_{ret}=0.1\ \mathrm{h}^{-1}$$

Justifications for these assumptions are driven by the need to replace some of the poorly identified rate constants (*i.e.* k_{C99} and k_{Ab}) with k_{del}, thus producing a model that was quite similar to a simple five compartment delay that was known to be sufficient to fit the labeling curves in subjects without plaques (Appendix A). The irreversible loss rate constant of APP was poorly identified (v_{APP}) and its effects were lumped into v_{C99}. It was further assumed that only half of C99 led to the production of Aβ38, Aβ40 and Aβ42. This is because Aβ peptides of other sizes are produced, with their abundance very roughly estimated from MALDI-TOF spectra of Aβ peptides in CSF [20]. It was further assumed that 50% of the irreversible loss of Aβ40 was to the CSF (*i.e.* $v_{40} = k_{CSF}$). Varying this fraction lost to the CSF between 10% and 90% had little effect on the results of the model (Appendix A). Finally, the return rate constant from the exchange compartment (k_{ret}) was set to 0.1 h^{-1}. This was optimized using the three participants with the largest extent of Aβ42 exchange, using different fixed values of k_{ret} and determining which value gave the best fit to the labeling curves (Appendix A). The six imposed relationships reduced the total number of parameters from 19 to 14 (because k_{C99}, v_{C99} and v_{40} were replaced by other parameters and v_{APP} and k_{ret} were set to specific values) and the number of independent parameters was reduced to 10 (an additional degree of freedom was lost by setting $k_{Ab38} + k_{Ab40} + k_{Ab42} = ½k_{del}$). Choice of the four dependent parameters is arbitrary, but calculation of k_{APP}, $k_{Aβ38}$, $k_{Aβ40}$ and $k_{Aβ42}$ from the other 10 parameters is illustrated in Appendix F. Exact solutions for the simplified model used in the previous publication are shown in Appendix G.

4. Results

4.1 System identifiability

Although development of the simplified model was described in section 3.6, the process was empirical. Using system identifiability analysis, a more rigorous approach is described here. The three transfer functions for the full model reveal that in principle 13 independent parameters may be determined from the labeling curve of each peptide (for methods, see references [11] & [12] and Appendix H). The full model has 25 parameters, demonstrating that the system is underdetermined. The assumptions from Section 3.5 of a common k_{CSF}, k_{ret} and k_{del} for the three peptides were physiologically based and reduced the number of parameters to 19. The following parameters appear together as sums everywhere within the transfer functions: $v_{38} + k_{CSF}$, $v_{40} + k_{CSF}$, $v_{42} + k_{CSF}$, $k_{C99} + v_{APP}$, and $k_{AB38} + k_{AB40} + k_{AB42} + v_{C99}$. This led to some of the assumptions of the simplified model, namely that k_{CSF} is a constant fraction of v_{40}, and that v_{APP} is zero. Additionally, if the sum $k_{AB38} + k_{AB40} + k_{AB42} + v_{C99}$ is replaced with the one parameter k_{Ab}, the number of parameters is reduced to 14. Recognizing that k_{APP} does not appear in the rate equations for fractional labeling reduces the number of parameters to 13. Thus, these assumptions make the problem ‘system

identifiable' [11]. The 24 algebraic equations that appear in the transfer functions were not further manipulated to demonstrate 'parameter identifiability' due to their complexity. Rather, 'practical identifiability' issues with the model are demonstrated by the sensitivity analysis below, further motivating the reduction from 13 to 10 parameters in the simplified model.

4.2. Sensitivity analysis

Sensitivity analysis of the simplified model would not yield information about k_{C99} and k_{Ab} because these were explicitly replaced by k_{del} in the solution. Thus, the exact solutions to the full model were utilized in the sensitivity analysis. Sensitivity analysis was performed using parameters from a PIB-negative non-carrier and a PIB-positive presenilin-1 mutation carrier. Both participants were of similar age. The parameter values for the simplified model were originally optimized using the measured hourly plasma leucine enrichment data as the input. To simplify the sensitivity analysis, all of the parameters in the simplified model were re-optimized using the mathematical functions f (Equation 3.2.1) to describe plasma leucine values. The differences between the raw hourly plasma leucine data and the f functions are shown in Figure 3A and 3C. The results of the parameter re-optimization are summarized in Appendix I.

The sensitivity analysis describes the sensitivity of the fractional labeling of Aβ42 in the third CSF compartment ($p_{Aβ42d3L}$) to changes in each of the major model parameters. For example, for k_{Ab42}, the sensitivity S_{kAb42} is:

$$S_{kAb42} = \frac{\partial P_{Ab42d3L}}{\partial k_{Ab42}} \quad \text{Eq(4.2.1)}$$

This is obtained by taking the partial derivative of the exact solution for $p_{Ab42d3L}$ (Eqn 3.3.8) with respect to k_{Ab42}. The sensitivity can be interpreted as:

$$\Delta p_{Ab42d3L} \approx \Delta k_{Ab42} \times \frac{\partial p_{Ab42d3L}}{\partial k_{Ab42}} \quad \text{Eq(4.2.2)}$$

for small Δk_{Ab42}.

For the sensitivity analysis, the exact solutions become unbounded when $k_{C99} \to k_{del}$ or $k_{Ab} \to k_{del}$. To overcome this, the derivatives with respect to each of the parameters was taken and then the limit of the resulting equations was evaluated as $k_{Ab} \to k_{C99}$ and then $k_{C99} \to k_{del}$, applying L'Hôpital's rule when necessary. The detailed methods are described in Appendix J.

Figures 5A and 5B show the sensitivity of $p_{Ab42d3L}$ to the various parameters, along with the measured and model $p_{Ab42d3L}$ (scaled by 6 for readability). The largest effect on $p_{Ab42d3L}$ was found with changes in v_{42}. Identical sensitivity was observed for k_{CSF}, because both rate constants describe irreversible loss of Aβ42 (see Equation 3.3.2). Within the first five hours of labeling, increases in v_{42} or k_{CSF} had no effect on $p_{Ab42d3L}$. This is expected, because of the delay in the appearance of Aβ42 in the final compartment. However, between hours 5 and 36, increased v_{42} or k_{CSF} leads to increases in the values of $p_{Ab42d3L}$ for the mutation

carrier, with a maximum effect immediately prior to the peak enrichment of Aβ42. For the non-carrier, increases in v_{42} or k_{CSF} also increased $p_{Ab42d3L}$, between hours 5 and 24, with a maximum effect about 2 hours prior to the peak enrichment of Aβ42. However, increases in v_{42} or k_{CSF} decreased $p_{Ab42d3L}$ between hours 24 and 36. The effects of increases in v_{42} or k_{CSF} on actual kinetic curves are shown in Figure 6A and 6B (for these figures, the rate equations were solved numerically, increasing one of the parameter values by 0.1 h^{-1} while holding all other parameters constant). Increasing v_{42} results in the labeling curve rising earlier, peaking higher, and falling more quickly. However, in the mutation carrier (Figure 6A), the quicker fall is halted after about 28 hours, likely due to the effects of the exchange compartment.

Returning to Figure 5, the next most important parameter that affected $p_{Ab42d3L}$ was k_{ex42}, the rate constant for entry of Aβ42 into the exchange compartment. An increase in this parameter lowered the peak $p_{Ab42d3L}$ and flattened the tail of the curve in both participants (Figure 6A and 6B). Increasing the rate constant for exit of Aβ42 from the exchange compartment (k_{ret}) led to increases in $p_{Ab42d3L}$ for the mutation carrier (Figures 5A and 6A), but this only became substantial after the peak in Aβ42 enrichment. As expected, k_{ret} had no effect with the non-carrier because no exchange was present in this participant ($k_{ex42} = 0$). The other parameters had only small effects on $p_{Ab42d3L}$, including k_{C99}, k_{Ab42}, k_{CSF} and k_{del} (k_{Ab42} and v_{C99} have identical sensitivities because both are constituents of k_{Ab}, which governs the irreversible loss of C99). Changes in the rate of irreversible loss of APP/C99 thus have much less of an effect on the Aβ42 labeling curve than the rate of irreversible loss of Aβ42 itself. Thus, substantial differences in labeling curves between subjects most likely reflect changes in the irreversible loss of Aβ42 and/or the presence of short term exchange, assuming that anatomical differences can be neglected.

The sensitivity of the FSR to parameter changes in the model parameters was also examined (Figure 7), which is simply the sensitivity of the time derivative of $p_{Ab42d3L}$ (*i.e.* the slope of the labeling curve). Using the parameter k_{Ab42} as an example, this is:

$$\frac{\partial}{\partial k_{Ab42}}\left(\frac{\partial p_{Ab42d3L}}{\partial t}\right)=\frac{\partial^2 p_{Ab42d3L}}{\partial k_{Ab42}\partial t}=\frac{\partial}{\partial t}\left(\frac{\partial p_{Ab42d3L}}{\partial k_{Ab42}}\right)=\partial S_{Kab42}\partial t \quad \text{Eq(4.2.3)}$$

Figures 7A&B shows the actual value of $\partial p_{Ab42d3L}/\partial$t around the upslope of the labeling enrichment curve (scaled by 10 for readability). The value of $\partial p_{Ab42d3L}/\partial$t varies considerably between 5-14 h, and resembles the result of fitting the middle portion of a sigmoidal curve to a straight line. Figures 7C&D show the *sensitivity* of $\partial p_{Ab42d3L}/\partial$t to changes in different parameters, and the measured $p_{Ab42d3L}$ and model $p_{Ab42d3L}$ in the region of the upslope are shown on all plots. For both participants, the largest effect on $\partial p_{Ab42d3L}/\partial$t (and thus FSR) came from v_{42} and k_{CSF}. The next largest effect on FSR was from k_{ex42}, which had an opposite effect from v_{42} and k_{CSF}. Thus, if both of these parameters are increased (as was noted in participants with plaques), they will tend to cancel each other out. The parameter k_{ret} had a modest effect on FSR, while the other parameters had even less effect.

The sensitivity of the monoexponential FCR was calculated (Figure 8), which is simply the sensitivity of the time derivative of the natural logarithm of $p_{Ab42d3L}$

$$\frac{dS^{log}}{k_{Ab42}} = ddk_{Ab42}\left(\frac{d\,ln\,(p_{Ab42d3L})}{dt}\right) = \frac{d}{dl_{Ab42}}\left(\frac{d\,ln\,(p_{Ab42d3L})}{dp_{Ab42d3L}}\frac{dp_{Ab42d3L}}{dt}\right) = \frac{d}{dk_{Ab42}}\left(\frac{1}{p_{Ab42d3L}}\frac{dp_{Ab42d3L}}{dt}\right) \quad \text{Eq(4.2.4)}$$

In Figure 8A, the actual $-\partial\ln(p)/\partial t$ for each participant is plotted. When $-\partial\ln(p)/\partial t$ is relatively flat, this indicates a good monoexponential fit. For the non-carrier, $-\partial\ln(p)/\partial t$ was relatively flat between 24-36 hours, the exact region used previously to determine the monoexponential FCR [7]. For the mutation carrier with plaques, however, the curve is not flat, meaning that it would not be fit as well by a monoexponential function. Overall, $-\partial\ln(p)/\partial t$ has a smaller mean value for the mutation carrier with plaques compared to the non-carrier, suggesting (incorrectly) decreased 'clearance' (*i.e*. irreversible loss) of Aβ42 in the mutation carrier with plaques compared to the normal control, when in fact irreversible loss is increased but masked by exchange.

The sensitivity of $-\partial\ln(p)/\partial t$ to changes in parameters is presented in Figure 8B&C, along with the measured $p_{Ab42d3L}$ and model $p_{Ab42d3L}$ scaled by 4 for readability. The sensitivity analysis on a log scale shows that increases in v_{42} or k_{CSF} lead to increases in monoexponential FCR (*i.e*. increases in $-\partial\ln(p)/\partial t$ between 24–36 hours), while increases in k_{ex42} would result in a decreased monoexponential FCR. The parameter k_{ret} had a complicated effect on $-\partial\ln(p)/\partial t$, decreasing monoexponential FCR up to 30 h, but increasing it after that. The parameters k_{Ab42}, v_{C99} and k_{C99} had nearly negligible effects on monoexponential FCR.

The goal of the isotope-labeling study was to determine k_{Ab42}, which governs the production rate of Aβ42, and ($v_{42} + k_{CSF}$), which govern the irreversible loss rate of Aβ42. The sensitivity analysis demonstrated that most of the variation in the Aβ42 labeling curve between subjects is likely due to differences in v_{42}, k_{CSF}, k_{ex42} and k_{ret}. However, k_{Ab42} may be reliably estimated because it has a large and direct effect on the concentration of Aβ42 in CSF. The sensitivity of the CSF Aβ42 concentration is the derivative of equation (3.5.6) with respect to the various parameters. For example, for k_{Ab42}:

$$S^{conc}_{Kab42} = \frac{\partial c_{Ab42d3L}}{\partial k_{Ab42}} = \frac{k_{CSF}k_{C99}k_{App}}{k_{del}\,(k_{C99}+v_{APP})\,(v_{42}+k_{CSF})}\left(\frac{1}{k_{Ab}} - \frac{k_{Ab42}}{k_{Ab}^{\,2}}\right) \quad \text{Eq(4.2.5)}$$

The sensitivity of Aβ42 CSF concentration to changes in the different parameters is presented in Table 1. The most important parameters that evoke changes in the CSF concentration of Aβ42 are k_{Ab42}, v_{42} and k_{CSF}. The production rate constant of Aβ42 from C99 (k_{Ab42}) was the most important parameter in determining the CSF concentration in the non-carrier, and second only to k_{CSF} in the mutation carrier. Increases in k_{Ab42} or k_{CSF} are predicted to result in increases in the CSF concentration of Aβ42, whereas an increase in v_{42} causes a reduction in CSF Aβ42 concentration because v_{42} represents shunting of Aβ42 away from the CSF. For this reason, the model predicts that CSF Aβ42 concentration is decreased due to shunting to irreversible loss, perhaps including deposition into plaques. Thus, most of the information about the rate of production of Aβ42 is provided by the

concentration of Aβ42 in CSF, while the shape of the isotopic enrichment curve tends to provide information about irreversible loss and exchange of Aβ42.

4.3 Effects of Scaling Factors and baseline correction

Sensitivity analysis is not helpful to analyze the effects of the scaling factors. However, the scaling factors affect the overall size of the fitted curve, which allows other parameters to be adjusted in combination to better fit different regions of the curve. Examining Figure 5, it is easy to imagine how changes in different parameter could reshape different parts of the curve. In Appendix K, the effects of removing the scaling factors are examined for both subjects. The parameters v_{38}, v_{40}, v_{42}, k_{CSF} appear to move in opposite directions from k_{C99}, v_{C99}, k_{Ab38}, k_{Ab40} and k_{delay}. In the mutation carrier with plaques, when the scaling factor is removed, the first group of parameters is increased and the second group decreases. The opposite occurs in the non-mutation carrier, probably because this subject had a scaling factor less than one, while the mutation carrier had a scaling factor greater than one. Interestingly, the production rate constant k_{Ab42} was increased in both subjects when the scaling factor was removed. The effects of baseline correction were also studied. The baseline was considered to be the first five time points, and their average was subtracted from all data points. Removing the baseline correction improved the fit for the non-mutation carrier only. Overall, the scaling factors might be needed due to instrument calibration errors, isotopic dilution or the presence of other processes not well-captured by the current model.

4.4 Relationship between production rate constants, irreversible loss rate constants, and CSF concentration

The *ratio* of production rate constants for Aβ42 relative to Aβ40 is simply Eq(3.5.6) divided Eq(3.5.5):

$$\frac{k_{Ab42}}{k_{Ab40}} = \frac{[A\beta_{42}]_{CSF}}{[A\beta_{40}]_{CSF}} \left(\frac{v_{42}+k_{CSF}}{v_{40}+k_{CSF}} \right) \quad \text{Eq(4.4.1)}$$

This shows that if the CSF concentration ratio of Aβ42:Aβ40 is to remain constant, increases in irreversible loss of Aβ42 relative to Aβ40 must be accompanied by increases in production of Aβ42 relative to Aβ40. However, if production is held constant and irreversible loss of Aβ42 relative to Aβ40 increases, as may occur in the presence of plaques, then the CSF concentration of Aβ42 relative to Aβ40 will decline, as has been observed [13]. This equation also shows that an increase in production without an increase in irreversible loss (perhaps due to an absence of plaques) should result in an increase in CSF concentration of Aβ42 relative to Aβ40. This has also been observed in mutation carriers that are much younger than their expected age of onset [13]. An important observation is that exchange of Aβ42 has no impact on the steady state CSF concentration, because the flux of mass into the exchange compartment is identical to the flux of mass out if at a steady state.

5. Discussion

The sensitivity analysis demonstrated that the overall shape of the Aβ labeling curves was affected by all of the parameters in the model, although some parameters had much larger effects than others. Previously, the FSR of the labeling curve between 5-14 hours was used to estimate production kinetics of Aβ peptides [7]. The sensitivity analysis demonstrates that the Aβ isotopic enrichment upslope is not highly affected by differences in production rate constants between subjects. Rather, the FSR likely reflected primarily irreversible loss and exchange, although no differences in FSR were found between Alzheimer's subjects and controls. However, in this region of the labeling curves, increased irreversible loss and increased exchange will tend to act in opposite directions, potentially canceling out each other's effects on FSR. On the other hand, as expected, the monoexponential FCR is strongly affected by the rate of Aβ irreversible loss in the absence of short-term exchange. However, the presence of exchange complicates the use of monoexponential FCR as a reliable measure of the true turnover rate. Much more information about the system is gleaned by fitting the entire time course to the new compartmental model, which is rooted in the biology and physiology of the system. In addition, the simultaneous use of CSF concentrations along with the labeling data allows determination of rate constants for both production and irreversible loss of Aβ peptides.

In other models, it was suggested that only the first fifteen hours of labeling data were required to fully describe the kinetics of the system [14]. While it is possible that the irreversible loss rate might be reasonably well estimated from the upslope of the labeling curve in normal participants, the current sensitivity analysis shows that the presence of exchange will affect the upslope of the curve, potentially muting the effects of increased irreversible loss (Figure 7C&D). Figure 2A illustrates that, in the mutation carrier, the largest difference between the Aβ40 and Aβ42 labeling curves occurs in the time period between about 19-30 h. Within this time frame, the effects of increased irreversible loss are declining, while the effects of exchange peak at about 19 h (Figure 5A&B). The sensitivity curve for v_{42} is not a perfect mirror image of that for k_{ex42} and thus analyzing the full time course is the best hope for separating out the effects of irreversible loss and exchange.

The FSR has also been used to analyze the effects of γ-secretase inhibitors on the labeling of Aβ peptides in humans and non-human primates [21, 22]. Large changes in the upslope of the labeling curves were noted. This is not inconsistent with the present analysis. Although the sensitivity of the FSR to changes in production rate constants is small, it is not zero. In the case of inhibition of γ-secretase, this should result in a large decrease in the production rate constants, resulting in a decrease in the FSR. As illustrated in Figure 4, FSR is in fact a measure of production, although it is affected by other parameters as well. The transient introduction of the γ-secretase inhibitors results in a non-steady state system, although the importance of the non-steady state nature of the system is difficult to estimate.

Several caveats about the compartmental model must be mentioned. Flow processes likely dictate the rate at which Aβ peptides transit from brain to the lumbar space. These processes are approximated here as a sequential series of compartments. More elaborate models that account for brain and subarachnoid space anatomy and flow may allow more accurate

determination of the rates of Aβ peptide irreversible loss and production. Thus, the sensitivities reported here are those of the current compartmental model, not of the underlying biological system, which has yet to be fully elucidated. The current dataset is also not rich enough to identify the rates of production and irreversible loss of APP and C99. Additional kinetic data relevant to the production and irreversible loss of APP and C99 would certainly improve the estimation of Aβ production and irreversible loss rate constants. Also, measurement of concentrations of various Aβ peptides has a large impact on the estimates of the production rate constants for the Aβ peptides, and improvements in the precision and accuracy of concentration measurements would greatly aid future studies.

6. Conclusions

We demonstrated rigorously that the FSR and monoexponential FCR previously used to characterize production and irreversible loss of Aβ peptides actually reflect the values of multiple parameters within a complicated system, and are not pure measures of production and irreversible loss. In steady-state studies, it is shown that estimation of the production rate is greatly enabled by combining isotope labeling data with concentration or pool sizes measurements. This also provides a mechanism for the observed decrease in CSF concentration of Aβ42 in Alzheimer's disease. The irreversible loss and exchange rate constants for Aβ peptides dominate the shape of the isotopic enrichment time course curve, and both constants may be readily determined by fitting the entire time course to the compartmental model. The later phases of the labeling process are better suited to resolve the irreversible loss and exchange processes of Aβ42. The conclusions of this study should enhance the design and interpretation of isotope-labeling experiments applied in the central nervous system.

Supplementary Material

Refer to Web version on PubMed Central for supplementary material.

Acknowledgements

We would like to thank John McCarthy for helpful discussions. This work was supported by funding from the NIH, R01 NS065667 (RJB) and P30 DK056341 (Nutrition Obesity Research Center, BWP).

Abbreviations

AD	Alzheimer's Disease
APP	Amyloid beta precursor protein
Aβ	amyloid beta
PET	positron emission tomography
PIB	Pittsburgh Compound B
CSF	cerebrospinal fluid
FSR	fractional synthesis rate

FCR	fractional clearance rate
FTR	fractional turnover rate
TTR	tracer-to-tracee ratio

References

1. Hardy J, Selkoe DJ. The amyloid hypothesis of Alzheimer's disease: progress and problems on the road to therapeutics. Science. 2002; 297:353–6. [PubMed: 12130773]
2. Haass C. Take five - BACE and the [gamma]-secretase quartet conduct Alzheimer's amyloid [beta]-peptide generation. EMBO J. 2004; 23:483–8. [PubMed: 14749724]
3. Bitan G, Kirkitadze MD, Lomakin A, Vollers SS, Benedek GB, Teplow DB. Amyloid beta -protein (Abeta) assembly: Abeta 40 and Abeta 42 oligomerize through distinct pathways. Proc Natl Acad Sci U S A. 2003; 100:330–5. [PubMed: 12506200]
4. Pellarin R, Caflisch A. Interpreting the aggregation kinetics of amyloid peptides. J Mol Biol. 2006; 360:882–92. [PubMed: 16797587]
5. Bateman RJ, Munsell LY, Morris JC, Swarm R, Yarasheski KE, Holtzman DM. Human amyloid-beta synthesis and clearance rates as measured in cerebrospinal fluid in vivo. Nat Med. 2006; 12:856–61. [PubMed: 16799555]
6. Wolfe, RR.; Chinkes, DL. Isotope Tracers in Metabolic Research: Principles and Practice of Kinetic Analysis. John Wiley & Sons; Hoboken, New Jersey: 2005.
7. Mawuenyega KG, Sigurdson W, Ovod V, Munsell L, Kasten T, Morris JC, et al. Decreased clearance of CNS beta-amyloid in Alzheimer's disease. Science. 2010; 330:1774. [PubMed: 21148344]
8. Elbert DL, Patterson BW, Ercole L, Ovod V, Kasten T, Mawuenyega K, et al. Fractional synthesis and clearance rates for amyloid beta reply. Nature Medicine. 2011; 17:1179–80.
9. Potter R, Patterson BW, Elbert DL, Ovod V, Kasten T, Sigurdson W, et al. Increased in vivo Amyloid-β42 production, exchange, and irreversible loss in Presenilin Mutations Carriers. Science Translational Medicine. 2013 Accepted.
10. Jankowsky JL, Fadale DJ, Anderson J, Xu GM, Gonzales V, Jenkins NA, et al. Mutant presenilins specifically elevate the levels of the 42 residue beta-amyloid peptide in vivo: evidence for augmentation of a 42-specific gamma secretase. Hum Mol Genet. 2004; 13:159–70. [PubMed: 14645205]
11. Cobelli C, DiStefano JJ 3rd. Parameter and structural identifiability concepts and ambiguities: a critical review and analysis. Am J Physiol. 1980; 239:R7–24. [PubMed: 7396041]
12. Bellman R, Astrom KJ. On Structural Identifiability. Mathematical Biosciences. 1970; 7:329–39.
13. Bateman RJ, Xiong C, Benzinger TL, Fagan AM, Goate A, Fox NC, et al. Clinical and Biomarker Changes in Dominantly Inherited Alzheimer's Disease. N Engl J Med. 2012; 367:795–804. [PubMed: 22784036]
14. Edland SD, Galasko DR. Fractional synthesis and clearance rates for amyloid beta. Nat Med. 2011; 17:1178–9. author reply 9-80. [PubMed: 21988985]
15. Ramakrishnan R. Studying apolipoprotein turnover with stable isotope tracers: correct analysis is by modeling enrichments. J Lipid Res. 2006; 47:2738–53. [PubMed: 16951401]
16. Zilversmit DB. The design and analysis of isotope experiments. Am J Med. 1960; 29:832–48. [PubMed: 13788500]
17. Patterson BW. Use of stable isotopically labeled tracers for studies of metabolic kinetics: an overview. Metabolism. 1997; 46:322–9. [PubMed: 9054476]
18. Bateman RJ, Wen G, Morris JC, Holtzman DM. Fluctuations of CSF amyloid-beta levels: implications for a diagnostic and therapeutic biomarker. Neurology. 2007; 68:666–9. [PubMed: 17325273]

19. Welander H, Franberg J, Graff C, Sundstrom E, Winblad B, Tjernberg LO. Abeta43 is more frequent than Abeta40 in amyloid plaque cores from Alzheimer disease brains. Journal of neurochemistry. 2009; 110:697–706. [PubMed: 19457079]

20. Portelius E, Andreasson U, Ringman JM, Buerger K, Daborg J, Buchhave P, et al. Distinct cerebrospinal fluid amyloid beta peptide signatures in sporadic and PSEN1 A431E-associated familial Alzheimer's disease. Mol Neurodegener. 2010; 5:2. [PubMed: 20145736]

21. Bateman RJ, Siemers ER, Mawuenyega KG, Wen G, Browning KR, Sigurdson WC, et al. A gamma-secretase inhibitor decreases amyloid-beta production in the central nervous system. Ann Neurol. 2009; 66:48–54. [PubMed: 19360898]

22. Cook JJ, Wildsmith KR, Gilberto DB, Holahan MA, Kinney GG, Mathers PD, et al. Acute gamma-secretase inhibition of nonhuman primate CNS shifts amyloid precursor protein (APP) metabolism from amyloid-beta production to alternative APP fragments without amyloid-beta rebound. J Neurosci. 2010; 30:6743–50. [PubMed: 20463236]

Highlights

- Sensitivity analysis of a compartmental model of amyloid beta kinetics
- Irreversible loss and exchange most readily identified by isotope labeling
- CSF concentration of amyloid beta reflects production and irreversible loss rates
- Limitations of previous kinetic analysis methods are described

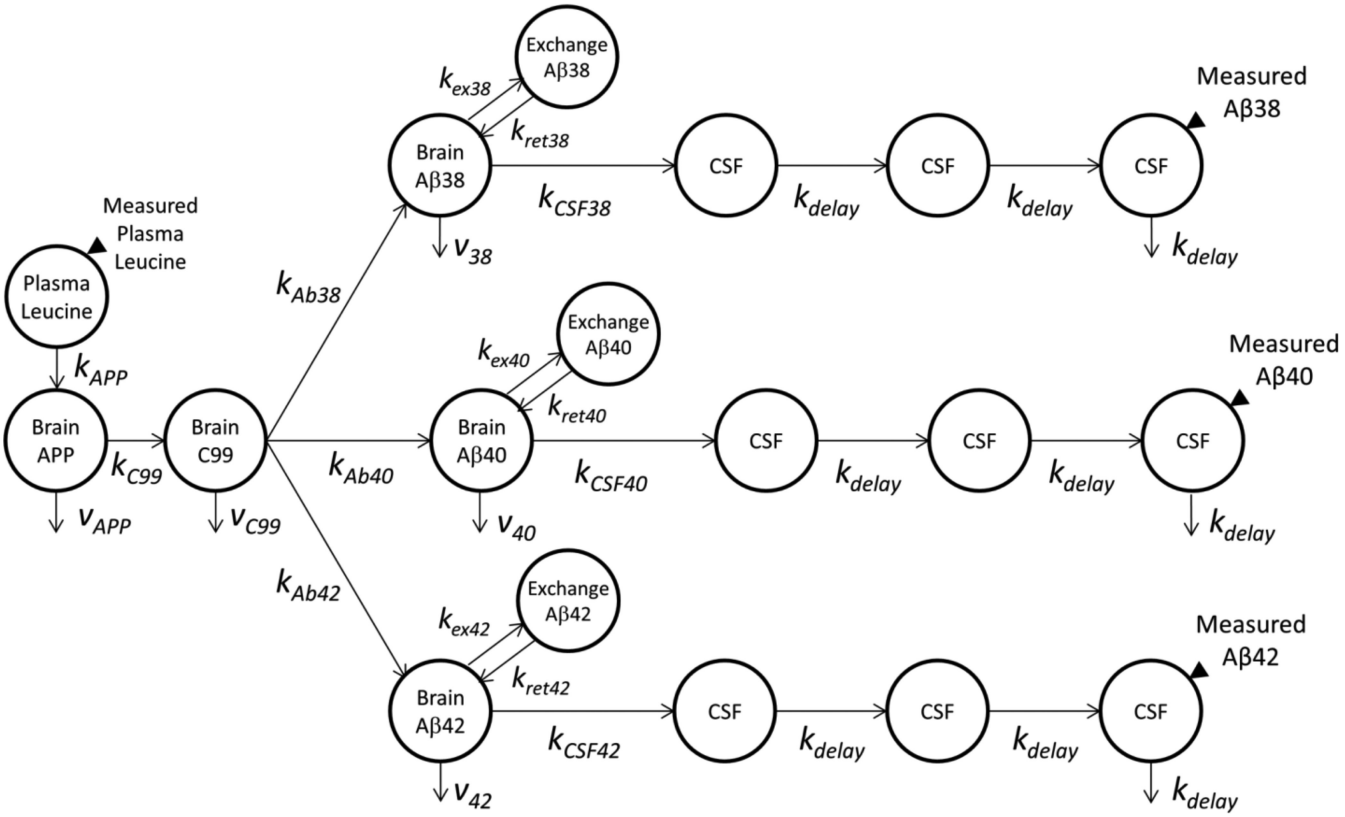

Figure 1.
Schematic of compartmental model

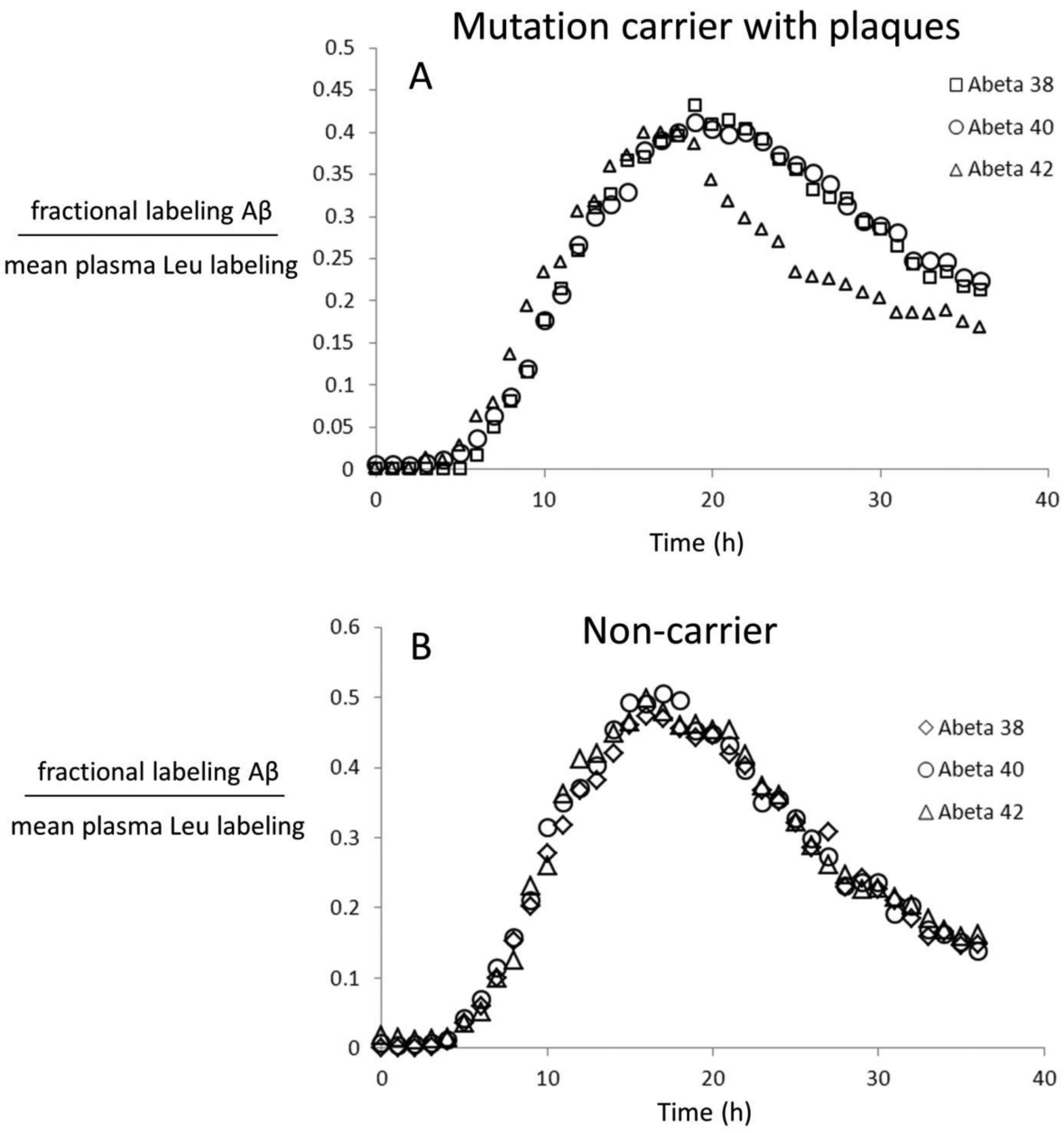

Figure 2. Morphology of Abeta isotopic labeling curves

Isotopically labeled leucine was infused into human volunteers for nine hours, while cerebrospinal fluid (CSF) was collected via lumbar puncture (spinal tap) hourly for 36 hours. The tracer-to-tracee ratio of Aβ peptides was measured by mass spectrometry and converted to fractional labeling of Aβ peptides. This was then normalized by the mean fractional labeling of leucine in blood plasma during the infusion period. (A) The Aβ42 isotopic labeling curve was markedly different from those of Aβ38 and Aβ40 in a presenilin-1 mutation carrier with amyloid plaques validated by PET PIB. (B) In a non-carrier without amyloid plaques, the isotopic labeling curves were similar for all three peptides. The averaged data for all study participants was published previously in reference [9].

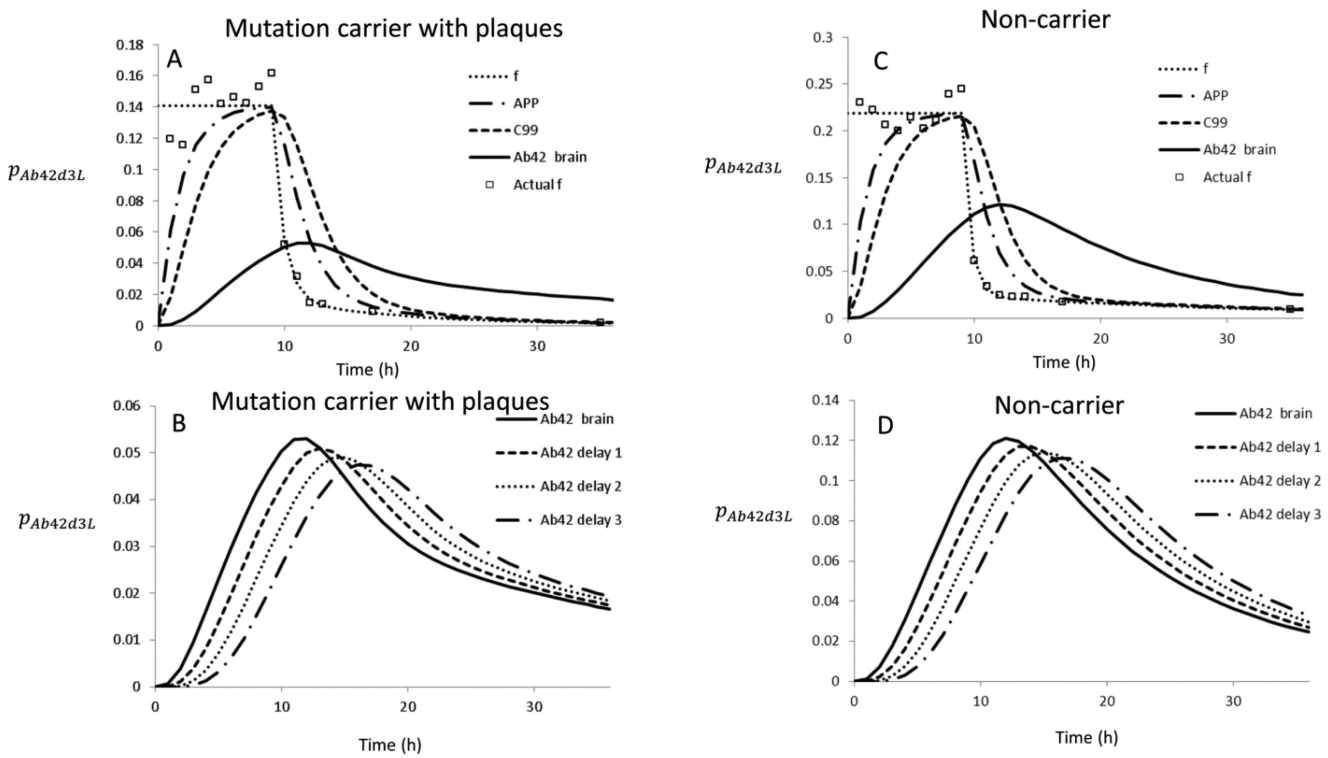

Figure 3. Predicted time course for Aβ precursors

The rate equations were solved numerically with re-optimized parameters listed in Appendix H for: (A&B) a presenilin-1 mutation carrier with plaques validated by PET PIB, and (C&D) a non-carrier without plaques. The predicted time course of plasma leucine, APP, C99 and Aβ42 in the brain compartment are shown in A&C. The predicted time course of Aβ42 in the brain, first delay compartment, second delay compartment, and third delay compartment are shown in B&D. The third delay compartment corresponds to the lumber sub-arachnoid space from which CSF was sampled.

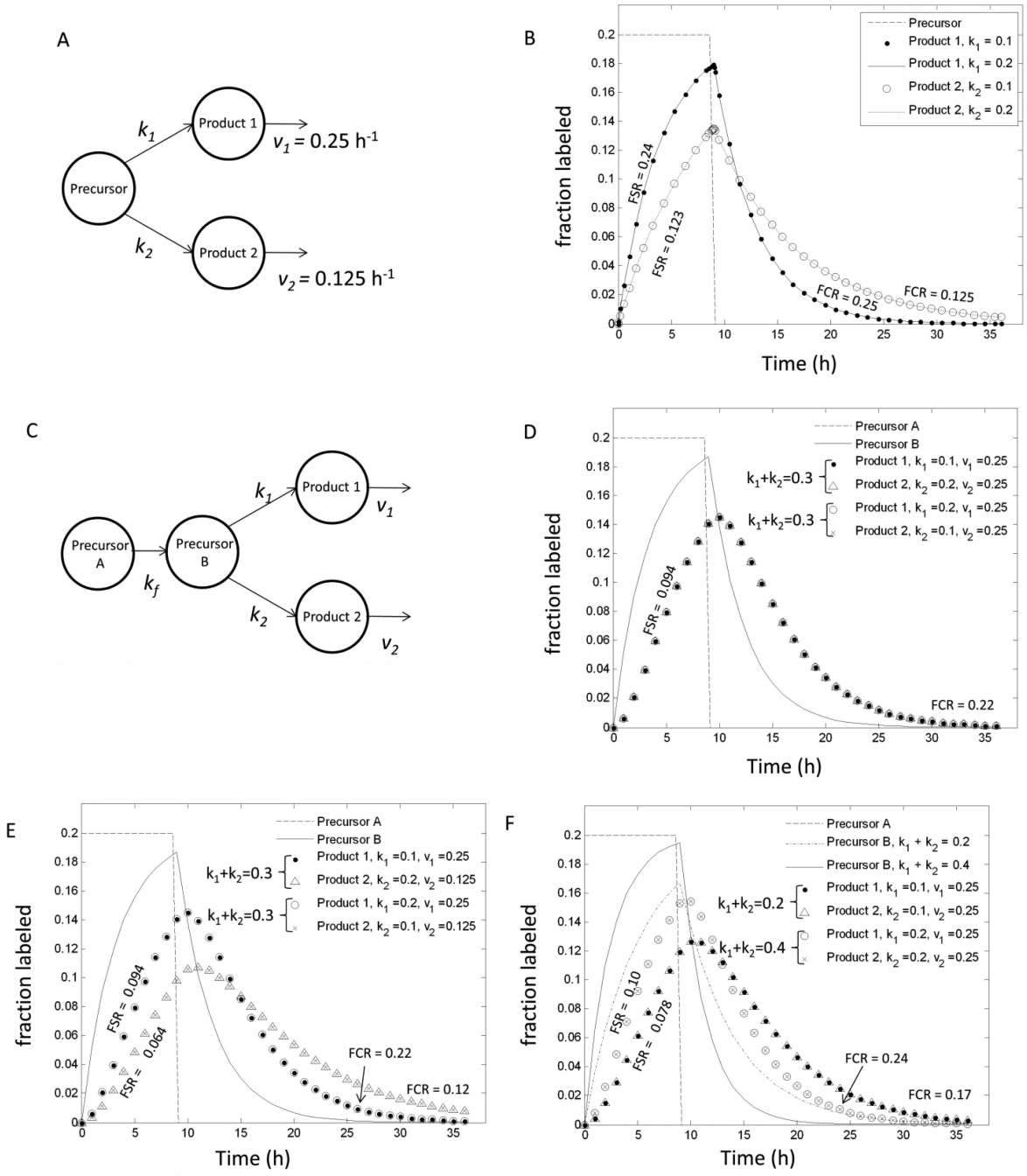

Figure 4. Fractional synthesis rate (FSR) and fractional clearance rate (FCR) for compartmental models with multiple pathways

(A) A simple model of a single precursor with constant labeling fraction during the labeling phase, which produces two products. (B) The labeling kinetics of each product show that variation of the production rate constants (k_1 & k_2) have no effect on labeling kinetics. Variation of the clearance rate constants (v_1 & v_2) has the only impact on labeling kinetics, and FSR and FCR are both provide good estimates of v_1 or v_2. (C) A two-step model in which precursor A is maintained at constant concentration during the labeling phase, but produces a precursor B, which then produces two products. (D) With v_1 & v_2 given the same

value, the values of k_1 & k_2 were set to different values, however, their sum remained constant. Regardless of the individual values of k_1 & k_2 the labeling curves for both products overlapped. FCR was close to but slightly lower than v_1 & v_2, while FSR was difficult to associate with any of the parameters. (E) The values of k_1 & k_2 were set to different values, however, their sum remained constant. The value of v_1 was set to twice that of v_2. Regardless of the individual values of k_1 & k_2 the labeling curves for each product overlapped. FCR was a close to but slightly lower than v_1 or v_2. FSR was 47% higher when the clearance rate constant was twice as large. (F) Production rate contants k_1 & k_2 were set equal to each other, but their sum was varied while setting v_1 & v_2 equal to each other. Changes in $k_1 + k_2$ led to distinct labeling curves. FCR approached the value of v_1 & v_2 when $k_1 + k_2$ became larger, but was much lower than v_1 & v_2 when $k_1 + k_2$ was lower. FSR increased by 28% when $k_1 + k_2$was doubled.

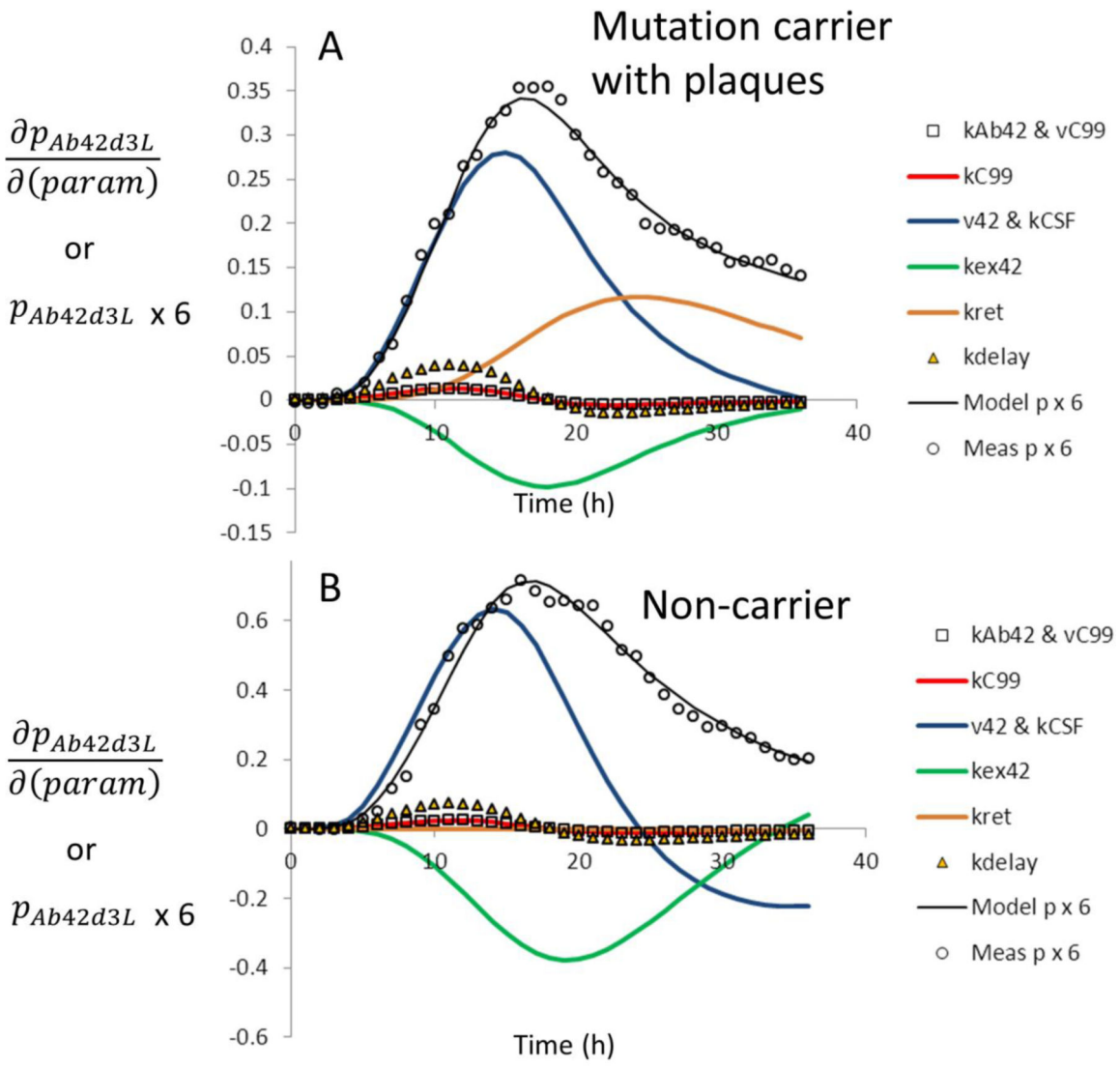

Figure 5. Sensitivity analysis of exact solution to the compartmental model

The rate equations corresponding to the compartmental model were solved analytically for the labeled fraction of Aβ42 in the third delay compartment ($p_{Ab42d3L}$), which corresponds to the fraction of labeled Aβ42 found in the lumbar CSF. The derivative of this function with respect to the listed parameters was taken and plotted as a function of time. Also plotted are the measured ('Meas p') and predicted ('Model p') fractional labeling, multiplied by 6 for readability. (A) Presenilin-1 mutation carrier with plaques validated by PET PIB scans, (B) Non-carrier without plaques.

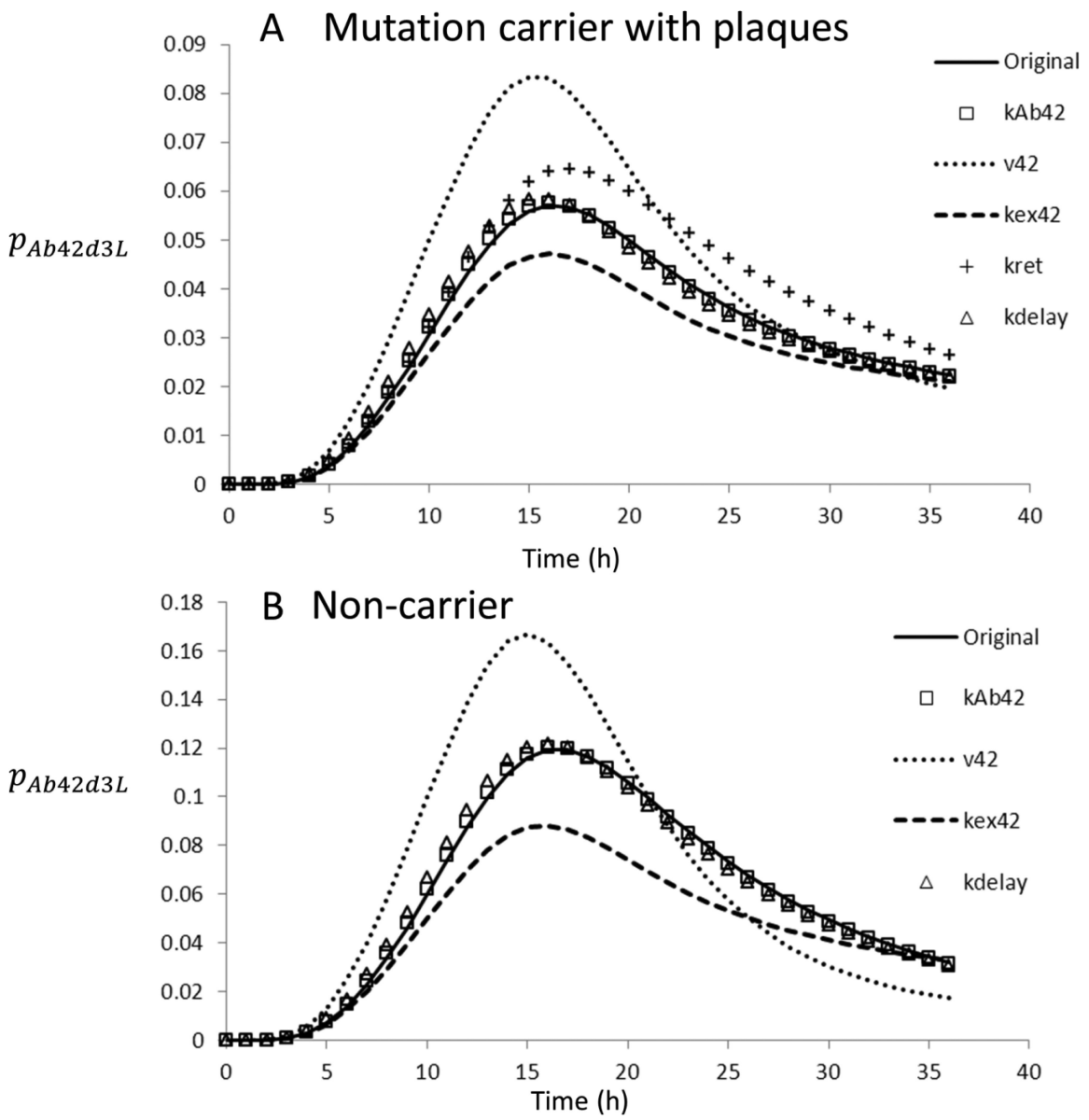

Figure 6. Changes in model predictions with changes in parameters

The indicated parameter values were increased by 0.1 h^{-1}. The rate equations were solved numerically with all other rate constants at their original values. (A) Presenilin-1 mutation carrier with plaques validated by PET PIB scans, (B) Non-carrier without plaques. The observed trends help to visualize the results of the sensitivity analysis shown in Figure 4.

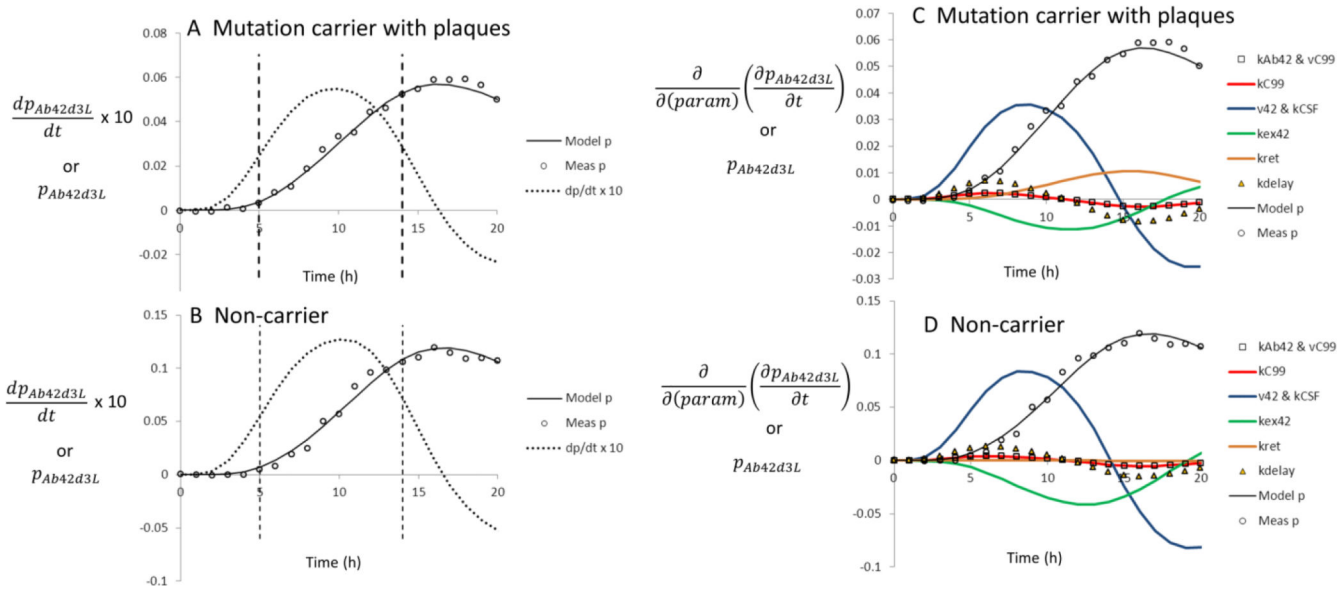

Figure 7. Sensitivity analysis of time derivative of exact solution

The time derivative of the labeling time course between 5 and 14 hours has previously been used to estimate production rate constants of kinetic systems (reference [7]). (A&B) 'Slope' of the labeling curve (d$p_{Ab42d3L}$/dt; multiplied by 10 for readability) shows that the data are not well-described by a straight line between 5 and 14 hours. (C&D) The sensitivity of d$p_{Ab42d3L}$/dt with respect to changes in the various parameters was evaluated. Also plotted are the measured ('Meas p') and predicted ('Model p') fractional labeling. (A&C) Presenilin-1 mutation carrier with plaques validated by PET PIB scans, (B&D) Non-carrier without plaques.

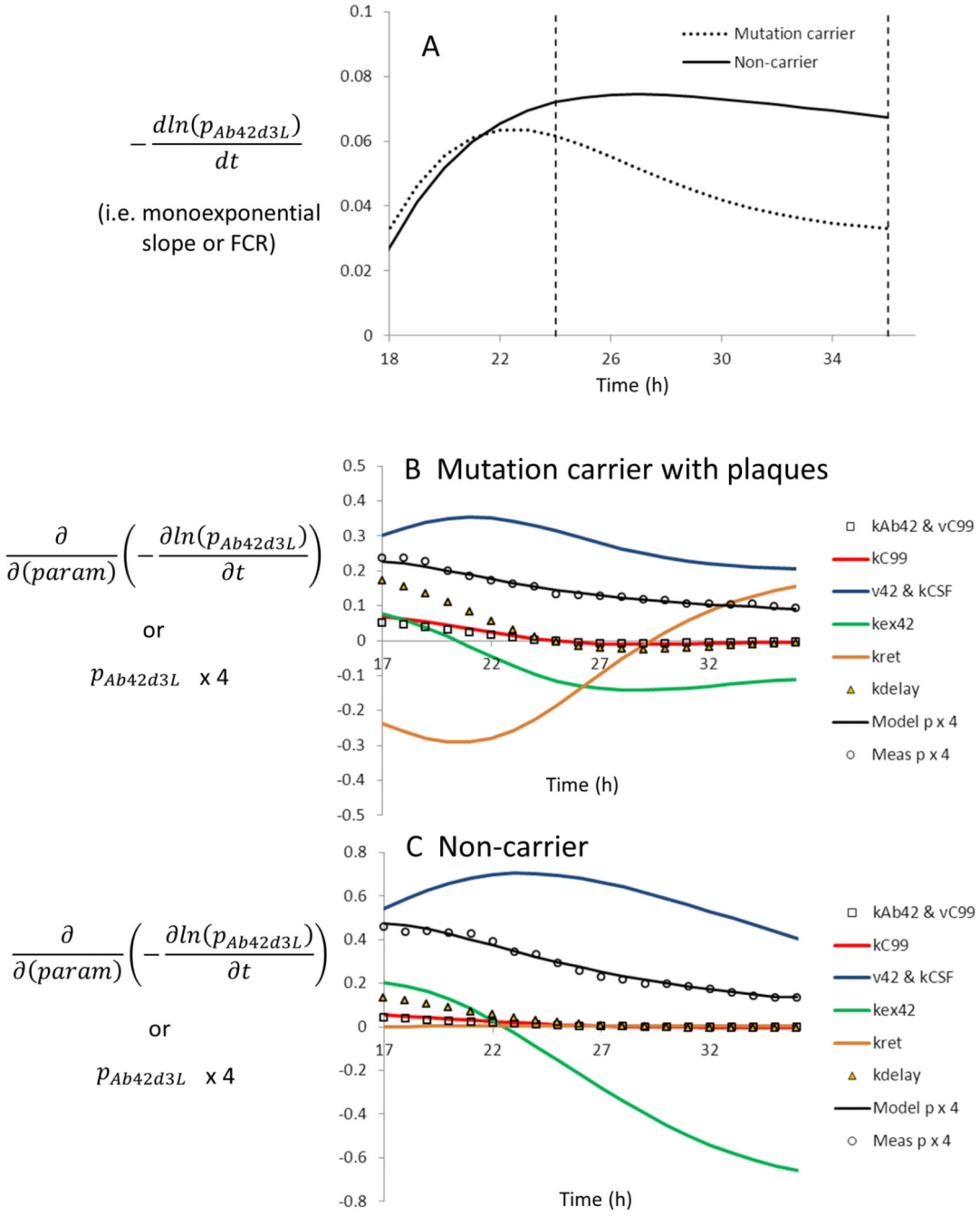

Figure 8. Sensitivity analysis of the monoexponential FCR

The time derivative of the logarithm of the labeling time course was previously used to estimate ‘clearance’ kinetics between 24 and 36 hours (reference [7]). (A) The time derivative of $-\ln(p_{Ab42d3L})$ is the instantaneous ‘monoexponential slope’ or FCR is shown for each subject. This is relatively constant for the non-carrier between 24 and 36 hours, but varies considerably for the mutation carrier. (B&C) The sensitivity of $d(-\ln(p_{Ab42d3L}))/dt$ to changes in parameter values was evaluated. Also plotted are the measured (‘Meas p’) and

predicted (‘Model p’) fractional labeling, scaled by 4 for readability. (B) Presenilin-1 mutation carrier with plaques validated by PET PIB scans, (C) Non-carrier without plaques.

Table 1

Sensitivity of CSF concentration of Aβ42 to changes in listed parameters

	Participant	
S^{conc} with respect to:	Mutation carrier	Non-carrier
k_{APP}	0.024	0.032
v_{APP}	−0.83	−1.4
k_{C99}	0	0
v_{C99}	−0.83	−1.4
$k_{Aβ38}$	−0.83	−1.4
$k_{Aβ40}$	−0.83	−1.395
$k_{Aβ42}$	12.7	30.7
v_{38}	0	0
v_{40}	0	0
v_{42}	−4.7	−9.6
k_{del}	−0.83	−1.4
k_{CSF}	14.3	8.8
k_{ex38}	0	0
k_{ex40}	0	0
k_{ex42}	0	0
k_{ret}	0	0